J. Fluid Mech. (1981), *vol.* 112, *pp.* 203–224
Printed in Great Britain

A unified two-parameter wave spectral model for a general sea state

By NORDEN E. HUANG, STEVEN R. LONG,
NASA Wallops Flight Center, Wallops Island, VA 23337
CHI-CHAO TUNG, YELI YUEN
North Carolina State University, Raleigh, NC 27650
AND LARRY F. BLIVEN
Oceanic Hydrodynamics, Inc., Salisbury, MD 21801

(Received 23 June 1980 and in revised form 25 February 1981)

Based on theoretical analysis and laboratory data, we proposed a unified two-parameter wave spectral model as

$$\phi(n) = \frac{\beta g^2}{n^m n_0^{5-m}} \exp\left\{-\frac{m}{4}\left(\frac{n_0}{n}\right)^4\right\}$$

with β and m as functions of the internal parameter, the significant slope § of the wave field which is defined as

$$\S = \frac{(\overline{\zeta^2})^{\frac{1}{2}}}{\lambda_0},$$

where $\overline{\zeta^2}$ is the mean squared surface elevation, and λ_0, n_0 are the wavelength and frequency of the waves at the spectral peak. This spectral model is independent of local wind. Because the spectral model depends only on internal parameters, it contains information about fluid-dynamical processes. For example, it maintains a variable bandwidth as a function of the significant slope which measures the nonlinearity of the wave field. And it also contains the exact total energy of the true spectrum. Comparisons of this spectral model with the JONSWAP model and field data show excellent agreements. Thus we established an alternative approach for spectral models. Future research efforts should concentrate on relating the internal parameters to the external environmental variables.

1. Introduction

As wind blows over the ocean, waves are generated. Their motions are random in nature; therefore any description of the wave field has to be of its statistical properties. Among the various statistical measures, spectral analysis is the most powerful means. The spectral function is not only important due to its own information content; it is needed also because various other statistical measures of the surface wave field are expressed either in terms of or by quantities derived from the spectrum (see, for example, Longuet-Higgins 1962). Thus, the spectral functional form becomes an urgently sought goal. However, because the wind-wave generation process is very complicated (see, for example, Phillips 1977), it is impossible to compute the spectral function

from the basic mathematical–physical laws. As a result, the void due to the lack of a spectral function has been filled in by various empirical or semi-empirical models.

Most of the recent spectral models can be traced to the common starting point of the spectral function proposed by Phillips (1958) who used dimensional analysis to derive the upper limit of the equilibrium or the saturation range spectral form. Thus $\phi(n)$ was expressed as

$$\phi(n) = \frac{\beta g^2}{n^5} \quad \text{for} \quad n \gg n_0, \tag{1.1}$$

which is sometimes approximated by

$$\phi(n) = \begin{cases} \dfrac{\beta g^2}{n^5}, & n \geqslant n_0, \\ 0, & n < n_0, \end{cases} \tag{1.2}$$

where β is a universal constant, g is the gravitational acceleration and n is the frequency in rad/s with n_0 as the frequency at the spectral peak. Later Pierson & Moskowitz (1964), based on equation (1.1) and some additional similarity analysis of Kitaigorodskii (1962), proposed a continuous functional model as

$$\phi(n) = \frac{\beta g^2}{n^5} \exp\left\{-\alpha\left(\frac{n_0}{n}\right)^4\right\}, \tag{1.3}$$

where

$$n_0 \simeq (0{\cdot}8 - 1{\cdot}0)\, g/U,$$

with α as an additional constant and U as the mean wind speed. Although some field and laboratory observations did provide data to support these models, there are still some difficulties in practical applications. In the first place, the spectral function, in general, models the high-frequency range better than that near the spectral peak where the energy is concentrated. But it is the energy content of the spectrum that is more important in applications. Secondly, the spectral models given in (1.2) and (1.3) are based on the physical conditions of equilibrium, i.e. a saturated or fully developed sea state. In the field, the area and duration of the sea that is fully developed is quite limited. Accordingly the usefulness of the models for fully developed sea are also limited.

The effort to find a generalized spectral function for the unsaturated sea culminated in the JONSWAP experiments where the spectra measured in fetch-limited (i.e. unsaturated or not yet fully developed) conditions were analysed extensively. It was found that the disagreement between JONSWAP data and the Pierson–Moskowitz model was indeed near the peak. Since this range for all practical purposes contains most of the energy, it is important to model it correctly. As a result of the experiment, Hasselmann *et al.* (1976) proposed the now well-known JONSWAP spectral model as

$$\phi(n) = \frac{\beta g^2}{n^5} \exp\left\{-\frac{5}{4}\left(\frac{n_0}{n}\right)^4\right\} \gamma^{\epsilon_n}, \tag{1.4}$$

where

$$\gamma = \frac{\phi(n)_{\max}}{\phi(n)^{\mathrm{PM}}_{\max}}, \quad \epsilon_n = \exp\{-(n-n_0)^2/2\sigma^2 n_0^2\}$$

and

$$\sigma = \begin{cases} \sigma_a, & n \leqslant n_0, \\ \sigma_b, & n \geqslant n_0, \end{cases}$$

with $\phi_{\max}^{\mathrm{PM}}$ as the spectral maximum derived from the Pierson–Moskowitz model, and, σ_a, σ_b are additional constants. This spectral model is basically the Pierson–Moskowitz model with an additional peak-enhancement function γ^{e_n}. When $\gamma = 1$, (1.4) reduces to (1.3) exactly. But the mean value of γ for all the JONSWAP experiment is around 3·3. In order to use (1.4), one will have to determine the five free parameters, all of which are given empirically as functions of the non-dimensional peak frequency, $\tilde{n}$, defined as

$$\tilde{n} = Un_0/g.$$

The significance of (1.4) is not that it fits data better. It should, because all the adjustable free parameters are determined by curve fitting. The real significance of (1.4) is that it is the first spectral function proposed for the unsaturated sea, while all the previous models are proposed for a fully developed sea only. Limitations on applying (1.4), however, still exist. In the first place, (1.4) contains numerous free parameters that cannot be determined *a priori*. Although empirical relationships reduce the parameters to two, the agreements between some of the empirical formulae and the data are rather crude, as shown by the statistical analysis summarized in Hasselmann *et al.* (1976). This makes the accuracy uncertain and application less convenient. Secondly, (1.4) is designed for the fetch-limited developing sea state cases only. Whether it also fits an unsaturated but decaying sea is more problematical. Nevertheless, the unsaturated spectral model offered by the JONSWAP experiments did open a new possibility of other spectral models for the non-saturated sea.

In this paper, we shall propose a new unified spectral model to represent the sea state under all stages of wave development and decay using only internal parameters. Although the data we used to derive the spectral form are collected in the laboratory, the analysis procedures used are based on dynamical considerations and are believed to be general in nature. Comparisons with published field results support this conclusion. Additional field experiments are being planned and the results of these will be presented later.

2. The proposed spectral model

The proposed spectral model is based on the laboratory data collected in the wind-wave–current interaction channel at NASA Wallops Flight Center. The detailed description of the laboratory facilities can be found in Huang & Long (1980). A group of spectra under various wind speeds are given in figure 1 (*a*) and a typical individual spectrum is given in figure 1 (*b*). From figure 1 (*a*), it is obvious that the saturated range upper limit as proposed by Phillips (1958) indeed exists. But this limit does not fit the individual spectra. Because our goal is to derive a model for the individual spectrum, we have to examine a typical spectrum in detail. Several features of this typical spectrum can easily be seen. First, the spectral bandwidth is usually very narrow. Secondly, the spectrum has a well-defined main peak and a secondary peak located at twice the peak frequency. Thirdly, the best-fitted envelope of the individual spectrum has a slope different, sometimes substantially so, from the generally accepted -5 law. This is especially true for the gentle wind cases ($u_* \leqslant 20$ cm s^{-1}). Finally, if we connect the main peak and the secondary peak by a straight line, it always provides us with a very good envelope of the whole high-frequency range.

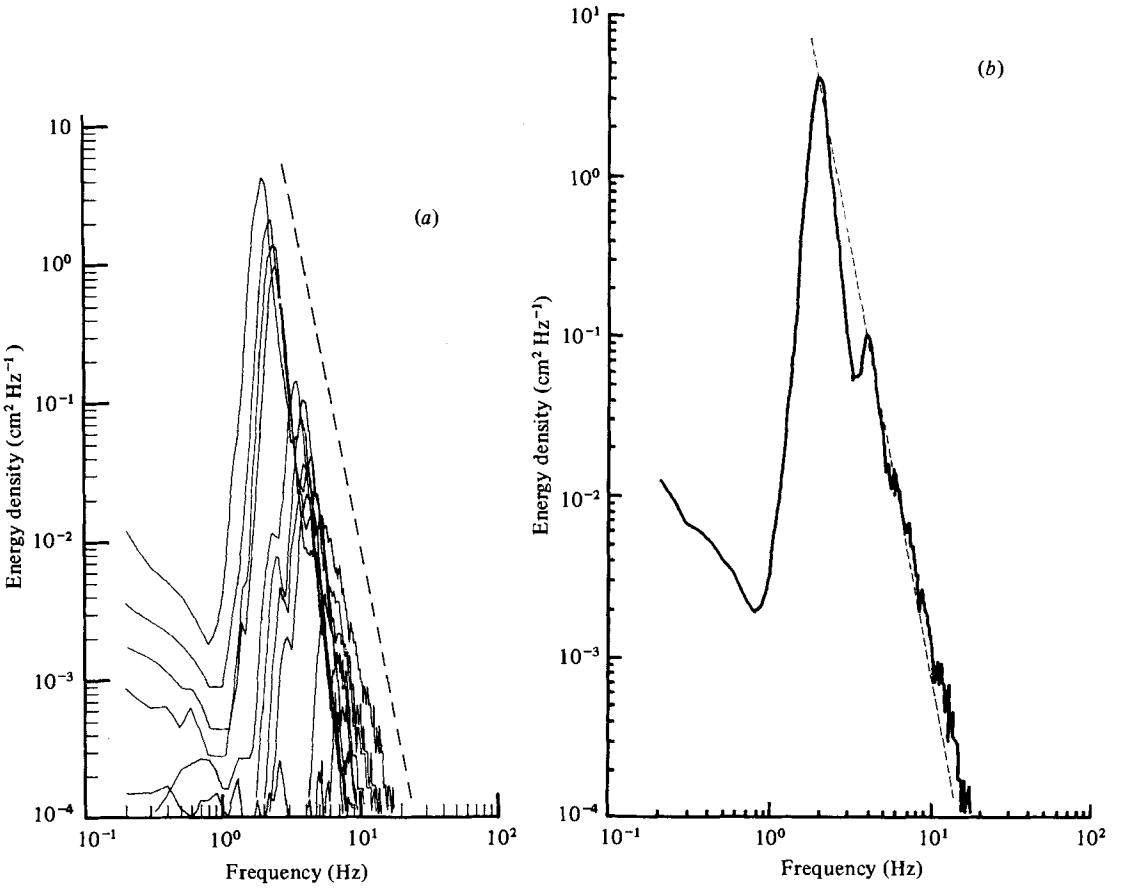

FIGURE 1. (*a*) A group of laboratory wind-wave energy spectra under different wind speeds. ---, indicates the -5 slope limit as proposed by Phillips (1958). (*b*) A typical laboratory wind-wave energy spectrum. The dashed line connects the primary and the second harmonic peaks to form an envelope of the high-frequency range.

The first feature is a generally accepted observational fact which enables us to use the narrow-band assumption in most of the statistical studies (see, for example, Longuet-Higgins 1957, 1962). The second feature is true for all the laboratory wave spectra. In the field, waves may be generated by different weather systems. Then the spectrum may have multiple primary peaks. We shall discuss these cases separately later in this paper. For the time being we shall concentrate on the single peak case. Even with a single peak, the second harmonics in the field spectrum may be less prominent than in the laboratory. This is because most waves in the field are not as steep and hence less nonlinear than the laboratory waves. Nevertheless the second harmonic peak does exist in all the carefully analysed data (see, for example, Kinsman 1960). The third feature reinforces the need for a peak-enhancement function; i.e. a slope of strictly -5 would not cover the range near the peak. Now if we use the line defined by the straight line connecting the main and the secondary peaks as the envelope, we can derive a closed form expression for its slope changes based on the dynamics of the wave motions. In fact, we can use a very simple model to prove that this secondary peak is the second harmonics according to the Stokes expansion. The proof can

be given as follows. Since the spectrum is narrow band, it follows that in the limit it can be approximated by a single train of waves. Using Stokes' expansion, we can write the surface elevation at a fixed location, $\zeta(x,t)$, as

$$\zeta(x,t) = a\cos\chi + \tfrac{1}{2}a^2k_0\cos 2\chi + \ldots, \tag{2.1}$$

where a is the wave amplitude, k_0 is the wavenumber and χ is the phase function. The frequency spectrum of this surface will have only two spikes located at n_0 and $2n_0$. The amplitudes of the spikes are proportional to a^2 and $(\frac{1}{2}a^2k_0)^2$. Consequently, the line connecting the two peaks will have a slope

$$m = \left|\frac{\log a^2 - \log(\frac{1}{2}a^2k_0)^2}{\log n_0 - \log 2n_0}\right| = \left|\frac{\log\left(\frac{2}{ak_0}\right)^2}{\log\frac{1}{2}}\right|. \tag{2.2}$$

For a narrow-band case as we have here, this approximation should work very well. For a broader band, the peak can be regarded as a collection of waves each having its own harmonics. Therefore, the slope of the line connecting the main and the harmonic peaks should still be governed by (2.2). However, for a random wave field, the amplitude should be substituted by the r.m.s. surface elevation, and k_0 by the wavenumber at the spectral peak. We thus make the substitution

$$\overline{(\zeta^2)}^{\frac{1}{2}} = \frac{a}{\sqrt{2}}, \quad k_0 = \frac{2\pi}{\lambda_0}. \tag{2.3}$$

With λ_0 above as the wavelength corresponding to the waves at the spectrum peak, then (2.2) can be written as

$$m = \left|\frac{\log(\sqrt{(2)}\,\pi\S)^2}{\log 2}\right|, \tag{2.4}$$

where the symbol § is called the significant slope of the wave field, defined as

$$\S = \frac{\overline{(\zeta^2)}^{\frac{1}{2}}}{\lambda_0}. \tag{2.5}$$

All the spectra from the laboratory data were used to test this relationship. The measured slope of the line connecting the main and the secondary peaks at twice the peak frequency is plotted as a function of § in figure 2, together with the curve defined by (2.4). The agreement is very good. This proves that the secondary peaks are indeed the second harmonics for Stokian waves.

If we push the waves to the limit of breaking, then we would have $a/\lambda = 1/14$ or § = 0·0505. Using this limiting value of §, we get $m = 4{\cdot}312$ from (2.4). This number is very close to the -5 law proposed by Phillips (1958). Laboratory data that we have obtained has never reached this limit. Under extremely high wind conditions ($u_* \geqslant 100$ cm s^{-1}, when all the waves are breaking violently and many water particles are airborne), the § value only reached 0·04 and the slope of the spectrum clustered near a limit of 5·5. As the wind decreased, waves became more gentle, and thus the § value decreased as well. The spectrum also became increasingly narrow. The measured m and the calculated value agree very well throughout all the range.

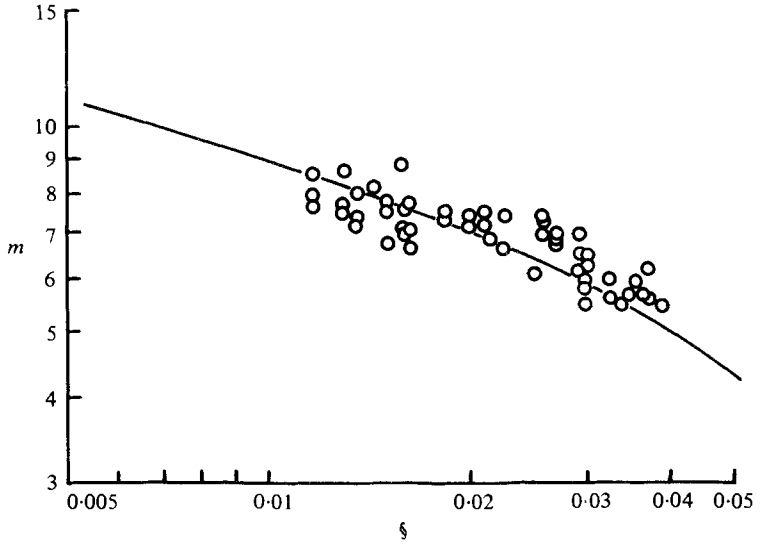

FIGURE 2. The slope of the high-frequency-range envelope defined by the line connecting the primary and second harmonic peaks as function of §. Solid line from equation (2.4).

The coincidence of the slope value approaching to the Phillips -5 law is very interesting. The fact that the empirically derived law based on dimensional analysis compares well with a simple calculation based on dynamical considerations is more than a pleasant surprise. In fact, we can show that the line connecting the main and the second harmonic peak should be the envelope, and therefore the limit is indeed near -5. Based on the nonlinear wave–wave interaction theory proposed by Phillips (1960) and extended to the random wave field by Hasselmann (1962, 1963*a*, *b*), the net effect of the nonlinear interaction is to shift the energy peak towards lower frequencies. This shift is incapable of generating prominent peaks on the high-frequency side of the spectrum. This is reinforced by the high rate of dissipation there. Consequently, on the high-frequency side, the only prominent peaks will be the higher harmonics resulting from the finite-amplitude effects of wave distortion. Field observations by Kinsman (1960) and theoretical calculations by Tick (1959) all confirmed these results. Thus, the line connecting the primary and second harmonic peaks should be the upper bound of the high-frequency spectrum range. Then equation (2.4) gives the maximum slope value as 4·312, a number extremely close to Phillips' dimensional analysis result. However, the sharper result based on dynamic considerations given in (2.4) offers a generalization of Phillips' -5 law. Thus we have a rule that will govern the shape of the high-frequency side of the spectrum under saturated as well as unsaturated seas.

Since § is a measure of wave slope, it is the indicator of nonlinearity of the waves. Thus the changing of the spectral shape with § agrees perfectly with the conclusion drawn by Hasselmann *et al.* (1976), who, after extensive comparisons between theoretical and experimental results, concluded that the shape of the spectrum is independent of the detailed distribution of the input and dissipation functions, and is controlled primarily by the nonlinear energy transfer.

Now let us restate how the result of this simple calculation can be used to explain what happens in the natural environment. Under strong wind and limited fetch, the

sea will grow. If the fetch is long enough, the sea state may become fully developed. But, prior to this saturated stage, the spectrum will not follow the Pierson–Moskowitz model. It may approach the fully developed spectrum by shifting the peak to lower frequency and broadening the bandwidth. As the waves propagate outside the storm area or as the storm dies off, the spectrum will become narrower and steeper. Since the shape of the spectrum is controlled primarily by the nonlinear energy transfer as concluded by Hasselmann *et al.* (1976), it is only logical to use the internal parameter § that measures nonlinearity to parametrize the spectral function. In this case, the wind speed, the duration, and the fetch all fade into the background. The integrated influence of all these external variables is reflected only in the geometric shape of the waves which in turn is measured by the parameter §. Thus we proposed an alternative approach for spectral models. Of course, the relationship between the internal parameters and the external variables is still lacking. Such a relationship is beyond the scope of this paper and should be the central problem of future research. Nevertheless, if one adopts the present approach, the necessary internal parameters can all be obtained from simple satellite observations. The details of this will be discussed later.

Based on these reasons, we proposed a new spectral model as

$$\phi(n) = \frac{\beta g^2}{n_0^5}\left(\frac{n_0}{n}\right)^m \exp\left\{-\delta\left(\frac{n_0}{n}\right)^\eta\right\}, \tag{2.6}$$

where β, δ and η are coefficient functions to be determined. The justifications of this basic form are as follows. We adopt

$$\beta g^2/n_0^5$$

to give the spectral function the correct dimensions. Since the slope of the high-frequency side is determined by m, we incorporate this as

$$(n_0/n)^m.$$

The last part is purely empirical to render the spectral function as a continuous function in an analytical form. This spectral function looks as if it contains five free parameters; two scale parameters β and n_0, and three shape parameters m, δ and η. But the parameters are not really free. Some of these can be determined explicitly.

Since n_0 is the frequency at the spectral peak, we should have

$$\frac{\partial\phi(n)}{\partial n} = 0 \quad \text{at} \quad n = n_0. \tag{2.7}$$

From (2.6) and (2.7) one can easily show that

$$m = \delta\eta. \tag{2.8}$$

If we choose $\eta = 4$ as did Pierson–Moskowitz (1964) and Hasselmann *et al.* (1976), then

$$\delta = \tfrac{1}{4}m. \tag{2.9}$$

Furthermore, by the definition of the spectral function, we have

$$\overline{\zeta^2} = \int_0^\infty \phi(n)\,dn. \tag{2.10}$$

By using the dispersive relationship of $n_0^2 = gk_0$ one can again show after some algebra that

$$\beta = \frac{(2\pi\S)^2 m^{\frac{1}{4}(m-1)}}{4^{\frac{1}{4}(m-5)}} \frac{1}{\Gamma(\frac{1}{4}(m-1))}, \tag{2.11}$$

with $\Gamma(\ )$ as the gamma function.

Because m is a function of $\S$ as shown in (2.4), and both δ and β are functions of m, it follows that three of the five parameters are reduced to a single parameter, $\S$. After we choose $\eta = 4$, the spectrum is determined by only two free parameters n_0 and $\S$. An alternative form of (2.6) is thus

$$\phi(n) = \frac{\beta g^2}{n^m n_0^{5-m}} \exp\left\{-\frac{m}{4}\left(\frac{n_0}{n}\right)^4\right\}, \tag{2.12}$$

with m and β given in (2.4) and (2.11) respectively. This spectral model is called the Wallops spectrum for future references.

3. Comparison of the Wallops spectrum with the JONSWAP spectrum and field data

Since the introduction of the JONSWAP spectrum, it quickly became the standard spectrum form in the field of wave research. To show how the Wallops spectrum compares with the JONSWAP spectrum and the field data should be very illustrative. For lack of the JONSWAP data or results in digital form, our comparison is limited to the published spectra in Hasselmann *et al.* (1976). In that paper four spectra from both hurricanes and open ocean cases are given as examples for comparison with the JONSWAP model. The spectra are all normalized by the value at the spectral peak. The functional form for the normalized Wallops spectrum is easily shown to be

$$\Phi(n) = \frac{\phi(n)}{\phi(n_0)} = \left(\frac{n_0}{n}\right)^m \exp\left\{-\frac{m}{4}\left[\left(\frac{n_0}{n}\right)^4 - 1\right]\right\}. \tag{3.1}$$

The comparisons of (3.1) with field data and the JONSWAP model together with the Pierson–Moskowitz model are given in figures 3(*a*, *b*, *c*, *d*) arranged in decreasing peak frequency. The agreement between the JONSWAP model and the field data is, of course, the best because the JONSWAP model is essentially a curve-fitting product with five free parameters to be adjusted. The Pierson–Moskowitz spectrum is uniformly overestimated. This is also to be expected because it is designed for the fully developed sea. These examples reiterate the fact that a fully developed sea is a rarity, because, even under hurricanes in the open ocean, the sea is still far from being fully developed.

The agreement between the Wallops spectrum and the field data is almost perfect for three out of the four cases. The case in which they do not agree very well is shown in figure 3(*a*), where several anomalies can easily be seen. First, the field spectrum has a low-frequency swell component. This swell peak could contribute to the total energy and make the r.m.s. elevation high, thus resulting in an artificially high value of $\S$. Those cases with multiple peaks will be discussed later. Secondly, the γ value for this spectrum is 6·04 which is also extremely high. This unusually high value of γ may suggest that this field data case needs careful re-examination.

A second comparison is made with the field data of Mitsuyasu *et al.* (1980) as shown in figure 4. The agreement is similar to that in the JONSWAP cases. In all fairness,

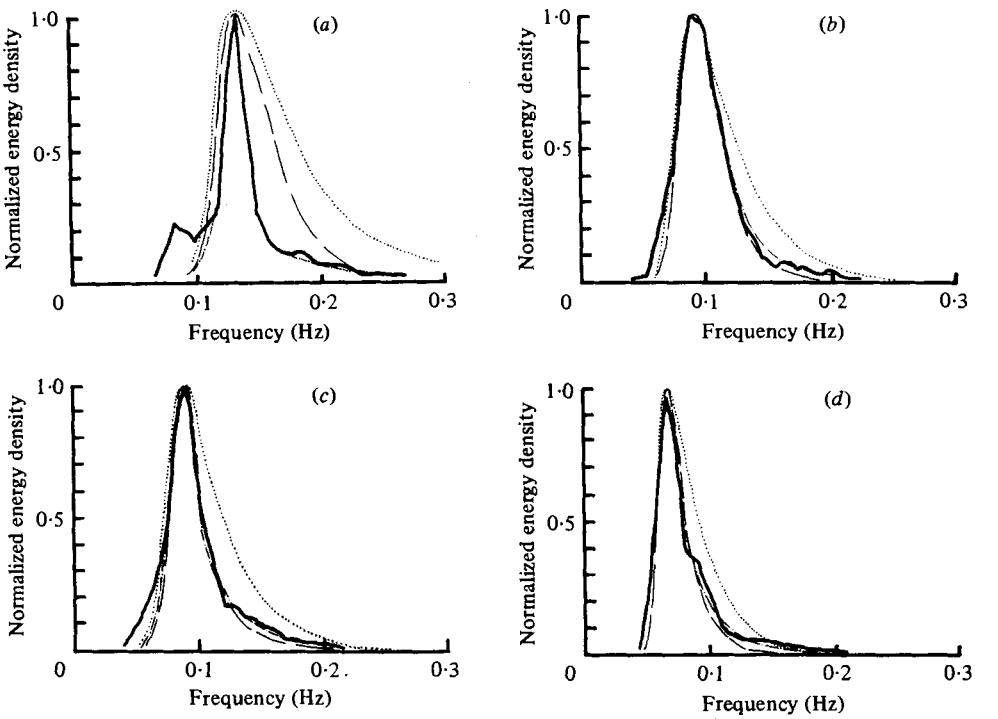

FIGURE 3. Comparisons of the Wallops spectrum (——), with the JONSWAP spectrum (–·–·–), the Pierson–Moskowitz spectrum (· · · · ·) and the field data (——). Spectra data from Hasselmann *et al.* (1976). (*a*) Argus Island, $n_0 = 0{\cdot}133$ Hz, § = 0·01145; (*b*) W. Atlantic, $n_0 = 0{\cdot}093$ Hz, § = 0·00815; (*c*) Hurricane Ava, $n_0 = 0{\cdot}087$ Hz, § = 0·0072; (*d*) Hurricane Camille, $n_0 = 0{\cdot}068$ Hz, § = 0·00625.

it should be pointed out that this comparison is not the best way to test the spectral models. This is because, by the normalization procedure, the β coefficient which determines the total energy level was left out. Furthermore, this normalization scheme also attached too much weight to the value of $\phi(n_0)$. An error of one point may significantly change the shape of the whole normalized spectrum. However, for lack of the true spectrum, these comparisons do offer some reference to the reality of the Wallops model which is derived based on detailed analysis of the laboratory data alone.

4. Some properties of the Wallops spectral model

The Wallops spectral model proposed here has much in common with the models used at the present time. It has the dimension similar to the Phillips (1958) saturation range spectrum; the analytic form of the Pierson–Moskowitz (1964) model; and the results similar to JONSWAP. In fact, when the energy-containing waves are approaching breaking, the m value decreases to the neighbourhood of 5. Then the Wallops model will reduce exactly to the Pierson–Moskowitz model. At that time, $\gamma = 1$ for JONSWAP. Then all three spectral models will be identical. The similarity stops here. There are a number of special properties that will set the Wallops model apart from not only the traditional form but also the traditional way of thinking.

First, the Wallops spectral model does not depend on the local wind condition.

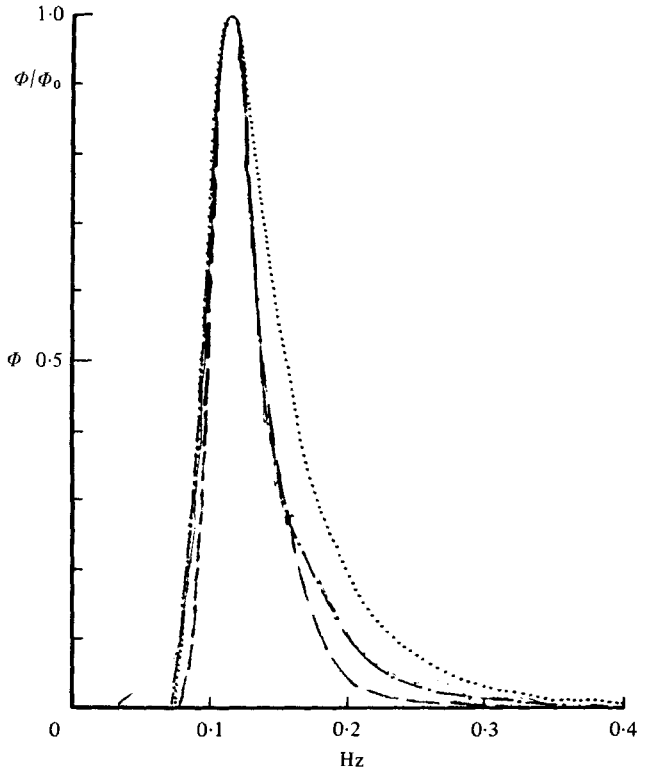

FIGURE 4. Same as in figure 3. Spectra data from Mitsuyasu *et al.* (1980). $E = 0{\cdot}5293\ \mathrm{m}^2, f_0 = 0{\cdot}112$ Hz.

Unlike Pierson–Moskowitz who related n_0 to mean wind or unlike JONSWAP where all the free parameters were related to $n_0 U/g$, the Wallops model depends on the internal parameters n_0 and §, the significant slope. From a theoretical point of view, our parametrization scheme can be justified along the lines of the conclusion of Hasselmann *et al.* (1976) discussed earlier in this paper. Intuitively, the justification can be presented as follows. Even though waves derive their energy from the wind, the fact remains that the water has a mass one thousand times that of the air. Once the energy is coupled into the water in the form of waves, the water waves have a much longer memory of what has happened. For example, as the waves propagate out of the storm area, the waves will still be high but the local wind can be rather low. An extreme case can be given by the experience of standing at the beach where waves always come toward the observer no matter what is the local wind direction. Of course, an ideal solution of the wave problem should be the one based on the physical laws. Then wind, fetch, duration, and the initial conditions will all be important parameters. Even then the ultimate integrated effect is still shown in the wave forms. The remaining problem for us is to find out the exact relationship between the internal parameters § and n_0 and the external variables. Short of that, using the wave form parameters is the only logical alternative and practicable way.

Secondly, the Wallops spectral model has reduced the necessity of empirically determined parameters to a minimum. Out of the five free parameters, three were determined by dynamical or analytical means which reduce β, δ and m to functions

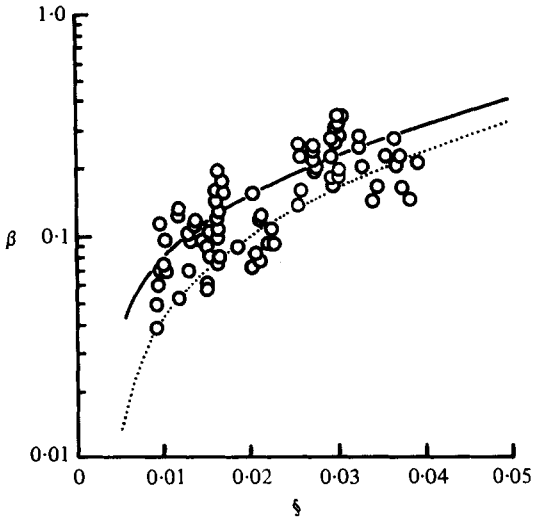

FIGURE 5. Comparison of the experimentally determined β, (○) with the calculated value from equation (2.11) (——) and equation (5.6) (· · · · ·).

of §. There is, however, one element of arbitrariness in the model, i.e. the value of η in (2.6) is set at 4 without any rigorous justification. At the present time, we can only argue that field observations seem to suggest this value. Additional study is needed here. Without any extensive field data at our disposal, we will leave it at 4. Future study may offer modifications that may improve the agreement between the data and the model.

Thirdly, the Wallops spectral model satisfies the total energy content of the spectrum automatically. Although the form of the Wallops model is similar to that of Pierson–Moskowitz, the coefficient β is not the Phillips constant. In general, it cannot even be used to make comparisons with the Phillips coefficient. A comparison of β values calculated from (2.11) with the laboratory data is shown in figure 5. The agreement of the values and the trend are excellent. An important consequence of the procedure used to determine β by (2.10) is that the spectrum automatically satisfies the total energy content requirements, i.e. the total area under the proposed spectrum is always equal to that of the true spectrum. This property is not guaranteed in any other spectral model where β is determined empirically, independent of energy considerations. Having had the total energy content correctly modelled, we are guaranteed a perfect agreement if the shapes also fit as in figures 3(*b*, *c*, *d*) and 4.

It should be pointed out that, under the special condition when m is fixed at the value of 5, then β would be the Phillips coefficient as in the Pierson–Moskowitz model. Then by (2.11), one would get

$$\beta = 5(2\pi\S)^2 = 20\pi^2\S^2. \tag{4.1}$$

This value can be easily shown to be in very good agreement with the JONSWAP data. In order to make a comparison between the formulae derived here and the observational data, we made a set of special measurements by forcing a -5 line on our spectra. β values are estimated from such fittings. The resulting values of β from our laboratory spectra are plotted in figure 6(*a*) together with the JONSWAP values

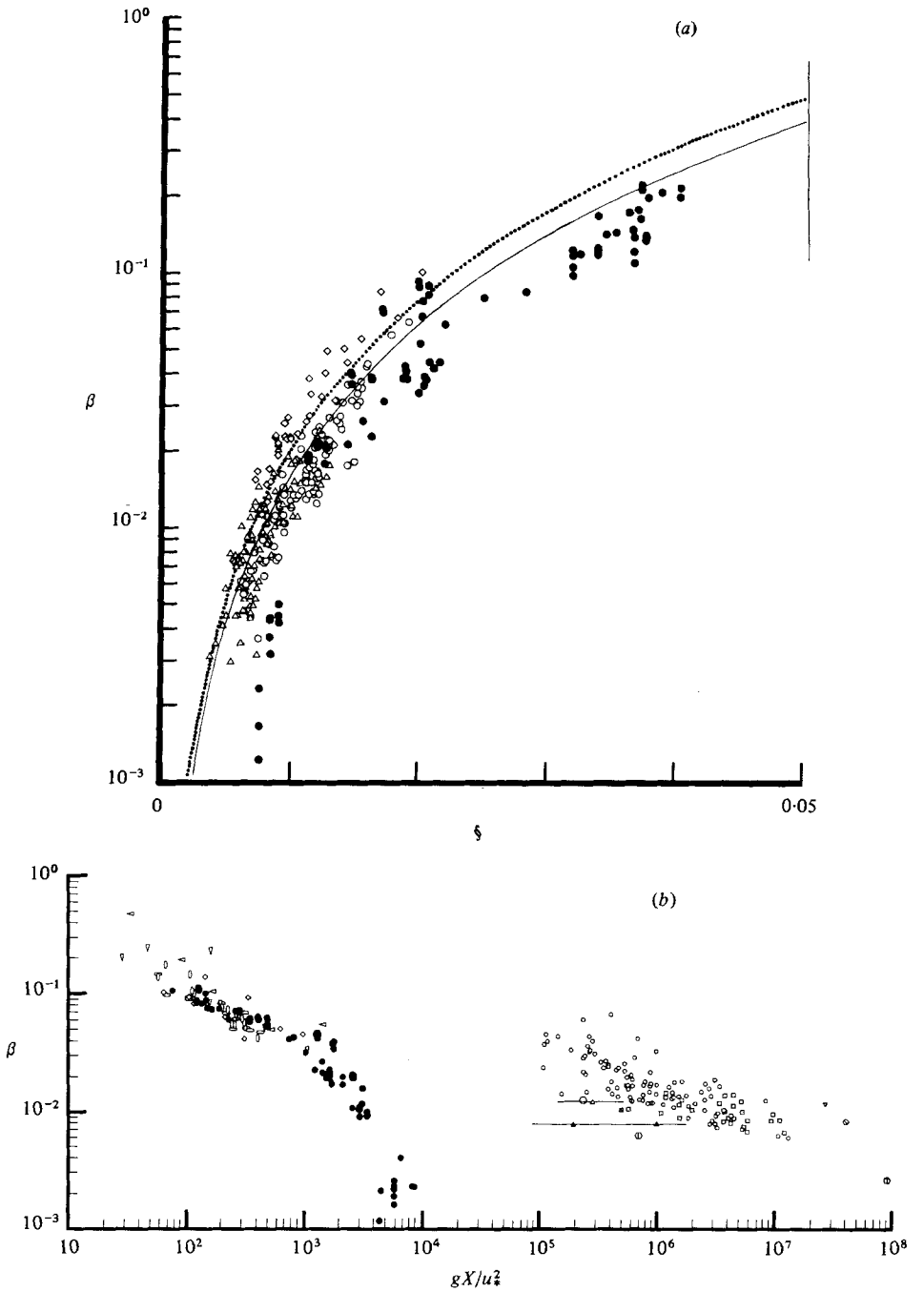

FIGURE 6. (*a*) The variation of the equilibrium range coefficient, β, with the significant slope, §. This study ●, JONSWAP data as reported by Müller (1976); ○, series A; △, series C; ◇, series E; solid curve $\beta = 16\,\pi^2\S^2$; dotted curve $\beta = 20\,\pi^2\S^2$. (*b*) The variation of the equilibrium range coefficient, β, with the non-dimensional fetch, gx/u_*^2. Laboratory results group to the left, field data to the right. ●, the present study; ▽, Toba (1973); ◁, Sutherland (1968); ⬭, Wu *et al.* (1977), average; ⬯, Wu *et al.* (1977), best fit; ◇, Mitsuyasu (1968), laboratory; ○, Hasselmann *et al.* (1973); □, Liu (1971); ⊘, Longuet-Higgins, Cartwright & Smith (1963); △, Burling (1959); ▽, Pierson (1962); ◈, Mitsuyasu (1968), Hakata Bay; ⬭, Hicks (1960); ⊠, Kinsman (1960); ⊕, Elliott (1972); ◬, Imasato (1976).

of β. The values of β as determined by equation (4.1) are shown. In general, the agreement is quite good, though it is not as good for the laboratory data as in figure 5. The subjective judgment in curve fitting may be the cause of the bias. Nevertheless, this comparison is still quite impressive in contrast to the parametrization scheme proposed by Hasselmann *et al.* (1976) and Wu, Hsu & Street (1977) where β was thought to be a function of the non-dimensional fetch as shown in figure 6(*b*). When considering the non-dimensional fetch, the field data and the laboratory data seem to fall into distinctly different clusters. It is not obvious how the two clusters can eventually merge smoothly even if the length of the laboratory channel could be extended to become comparable with some of the field cases conducted in lakes or enclosed bays (for example, Burling 1959 or Kinsman 1960). Although attempts have been made to draw a straight line through the points, as found in Hasselmann *et al.* (1976) and Wu *et al.* (1977), the fit is not really impressive. Such curve fitting also ignores the existing trend within each individual cluster. Faced with the evidence presented here, we feel that parametrization of β by such empirical formula in terms of the non-dimensional fetch should be abandoned. In fact, one of the best-fitted curves in the JONSWAP results is

$$\frac{\tilde{E}\tilde{f}_m^4}{\beta} = 1{\cdot}6 \times 10^{-4}, \tag{4.2}$$

where

$$\tilde{E} = \frac{\overline{\zeta^2} g^2}{U^4}, \quad \tilde{f}_m = \frac{f_m U}{g}, \tag{4.3}$$

in which U is the mean wind speed and f_m is the frequency at the spectral peak in Hz. The β is the equilibrium coefficient function. If we combine (4.2) and (4.3), and with the help of the dispersion relationship, we would get

$$\beta = 16{\cdot}04\pi^2 \S^2. \tag{4.4}$$

This value is very close to that given in (4.1) which resulted from m being fixed at $m = 5$.

These results further demonstrate the advantages of the internal variable parametrization scheme as compared with the conventional external variable parametrization approach in spectral function modelling.

It should be emphasized that this comparison is only meaningful if we force the spectrum to an $m = 5$ value as was done in Pierson–Moskowitz and JONSWAP. The agreement of the β value with the JONSWAP data at $m = 5$ should not be used as evidence to prove the m value should be fixed at 5. When $m = 5$, we have the Pierson–Moskowitz model or the JONSWAP model without the peak enhancement function. It is, however, unlikely that m will approach 5 in the field. The examples in figures 3(*a*, *b*, *c*, *d*) and 4 are all from open ocean and some even under hurricanes. But none of the cases have an m value anywhere near 5. On the other hand, it should also be pointed out that the present result should not be used to disprove the Phillips -5 law either. Enough evidence, both from laboratory and the field, indicates that the spectral shape indeed follows n^{-5} for $n \geqslant 2n_0$ for some cases. But, invariably, the energy content in such a range is always negligible. The point we want to make here is to model the energy-containing part of the spectrum. This spectral model may not work as well as Phillips' saturated range spectrum and its derivatives at the high-frequency

range. But it is believed to offer a superior alternative for the cases when the energy content is the critical consideration.

Fourthly, the Wallops spectral model maintains a variable bandwidth. Spectral bandwidth is not only an important measure of the spectral shape, but also the crucial parameter to determine the group length of the wave packets (see, for example, Longuet-Higgins 1976, 1962). To discuss the spectral bandwidth, we have to define the moments of the spectrum. Let the ith moment of the spectrum, M_i, be defined as

$$M_i = \int_0^\infty n^i \phi(n)\, dn. \tag{4.5}$$

Then

$$M_0 = \overline{\zeta^2} = \frac{\beta g^2 4^{\frac{1}{4}(m-5)}}{m^{\frac{1}{4}(m-1)} n_0^4} \Gamma\left(\frac{m-1}{4}\right). \tag{4.6}$$

In general, one can show that

$$M_i = M_0 \left(\frac{m}{4}\right)^{\frac{1}{4}i} n_0^i \frac{\Gamma(\frac{1}{4}(m-i-1))}{\Gamma(\frac{1}{4}(m-1))}. \tag{4.7}$$

Let us follow Longuet-Higgins (1957) to define the spectral bandwidth, ν, as

$$\nu^2 = \mu_2 / M_2, \tag{4.8}$$

where μ_2 is the second central moment of the spectrum, i.e.

$$\mu_2 = \int_0^\infty (n - \overline{n})^2 \phi(n)\, dn,$$

with $\overline{n} = M_1/M_0$ as the mean frequency. Then we can show, after some algebra, that

$$\nu = \left\{1 - \frac{\Gamma^2(\frac{1}{4}(m-2))}{\Gamma(\frac{1}{4}(m-3))\,\Gamma(\frac{1}{4}(m-1))}\right\}^{\frac{1}{2}}. \tag{4.9}$$

Since m is a function of §, clearly ν is a function of § alone. Thus the present model gives a spectrum of variable bandwidth depending upon the nonlinearity of the waves in the field.

If we fixed $m = 5$, we would get a fixed value of ν at 0·468 for the Pierson–Moskowitz spectrum. If we use the simpler spectrum as given in (1.2), we would have $\nu = 0{\cdot}35$. The ν values of all the available spectra from the laboratory are plotted in figure 7 together with the calculated value from (4.9). The agreement between the data and the model function is not exact, but the trend is unmistakable. Neither the Pierson–Moskowitz nor the simpler spectrum in (1.2) can model the trend as shown in figure 7. Unfortunately, we do not have the digital form of the JONSWAP spectra data, otherwise such a direct quantitative comparison would be most interesting. However, based on the agreement of the spectral shape on visual inspection, the agreement in bandwidth between field data and our model is to be expected.

Since the bandwidth is the parameter to determine the group length, we will try to calculate the group length, which has very important practical applications. According to recent observations, most of the damage to ships and ocean engineering installations is caused not by a single big wave, but by the combination of the big waves coming in groups. The mean number of waves in a wave group was calculated by Longuet-Higgins (1962) as

$$N = \left(\frac{e}{2\pi}\right)^{\frac{1}{2}} \frac{1}{\nu}. \tag{4.10}$$

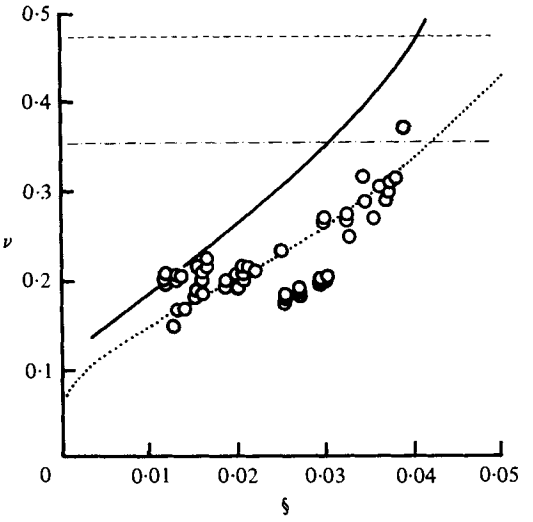

FIGURE 7. Comparison of the experimentally determined bandwidth parameter ν (○) with that of the Pierson–Moskowitz spectrum (– – –), the Phillips spectrum given in equation (1.2) (–·–·–), the full Wallops spectrum (——), and as determined by equation (5.7) (· · · · ·).

If we use the Pierson–Moskowitz spectrum, all the groups will contain exactly the same mean number of waves. And each group will have 1·5 waves in the mean. If we use the present model with the variable bandwidth, the group length will vary from one sea state to another depending on the significant slope of the wave field. The four spectra given in figures 3(a, b, c, d) give a mean value of $\S = 0{\cdot}0083$ which will generate a $\nu = 0{\cdot}16$. Then equation (4.10) gives $N = 4$, a number very suggestive of the common folklore that every fourth (or seventh) wave is the highest.

The calculated bandwidth can also be used to justify the narrow-band approximation used earlier. The narrowness of the spectrum can be regarded as a consequence of the weak nonlinear wave–wave interaction (see, for example, Phillips 1977). According to the nonlinear interaction theory of Hasselmann (1962, 1963a, b), the energy transfer between different wave components are weak in general. The net effect is to make the flow of energy occur from the high-frequency to the low-frequency components. Consequently, whatever energy was transferred would be concentrated near the peak. Additional energy would be dissipated in breaking. Thus all spectra show a prominent peak and a sharp frontal face which satisfies the narrow-band approximation very well.

Finally, we have to address the complicated case of multiple peaks. Such cases are commonly generated by different weather systems. The present spectral model cannot handle this case easily, nor can the earlier ones. However, if we use the fact of weak interaction, we can apply the principle of superposition to decompose the given wave field into independent sub-fields from each storm system. The proposed spectrum model will be applicable to each sub-field and the algebraic sum will be the final answer. This answer would be an approximation only. However, this approximation would be highly accurate because of weak nonlinear interactions.

5. An application of the Wallops spectrum

The inputs to initiate the spectrum are quite unconventional. The two internal parameters n_0 and §, however, are not difficult to obtain. Routine field observations give the significant wave height (which is related to $\overline{\zeta^2}$), and dominant frequency (which is n_0). With these two quantities, we can calculate the significant slope with the help of the dispersive relationship, and then define the spectrum.

An alternative and a more desirable way of defining the spectrum is to use the remote sensing method. Specifically, we can derive all the necessary parameters from a radar altimeter. A radar altimeter is a narrow-beam, pulsed, nadir-directed radar. The measurement of the total travel time between the satellite and surface determines the altitude of the satellite. When the radar pulse is reflected from the ocean surface, the return pulse shape contains the information of the probability distribution of the wave height (McGoogan 1975). Therefore, by processing the return pulse data, we can get not only the r.m.s. wave height (Parsons 1979), but also other statistical properties such as the skewness of the surface wave elevation distribution. This coupled with the results by Huang & Long (1980) which showed that

$$K_3 = 8\pi\S = 8\pi\frac{(\overline{\zeta^2})^{\frac{1}{2}}}{\lambda_0}, \tag{5.1}$$

one can actually get the § and n_0 (calculated from λ_0) from the altimeter data. The feasibility of this approach was established by Walsh (1979). Thus once an altimeter is available, the data will enable us to calculate wave spectra directly. However, the key link between the satellite data and the extraction of the necessary information for the eventual applications is based only on an empirical relationship derived from laboratory and very limited field data by Huang & Long (1980). Although comparison between (5.1) and available data showed good agreement, it would be highly desirable to find a rigorous theoretical guide for this result so that (5.1) can be used with confidence.

The theoretical groundwork has actually been previously done by Longuet-Higgins (1963). He showed that the skewness can be expressed in terms of the directional spectrum in a complicated convolution form. Because such a form is impractical if not impossible for routine calculation, he further established the limits of the skewness in terms of the one-dimensional frequency spectrum only. The theoretically derived limits of the skewness are given by

$$0{\cdot}44L \leqslant K_3 \leqslant 1{\cdot}01L, \tag{5.2}$$

with

$$L = I/(\overline{\zeta^2})^{\frac{3}{2}}.$$

The quantity I is given by

$$I = 12\int_0^\infty \left[\int_0^{n'} k\phi(n)\,dn\right]\phi(n')\,dn', \tag{5.3}\dagger$$

† These expressions were independently checked by us using an integral representation of the surface wave field as in Huang & Tung (1976). The results are identical with those derived by Longuet-Higgins (1963). Recently D. Barrick and F. Jackson (private communications) both pointed out that the expansion of surface elevation in Longuet-Higgins (1963) will not reduce to the classical Stokes waves for a delta-shaped spectrum. According to their derivations, the result is a factor of 2 smaller than (5.2). A similar factor of 2 discrepancy also existed in the non-linear effect on phase velocity in a random wave field as reported by Huang & Tung (1976). Further investigation on this point is needed.

where $\phi(n)$ is the frequency spectrum, k is the wavenumber and n is the frequency in rad/s. Comparisons between (5.2) calculated numerically and the experimentally determined skewness based on Kinsman (1960) were made by Longuet-Higgins (1963). The agreement was very good. This indicated that the bounds given in (5.2) are indeed reasonable limits. However, even in the reduced form of (5.2) and (5.3), the limits are still inconvenient for applications. In order to evaluate L, one will have to calculate I, which still includes convolution of the frequency spectrum. Then, it becomes almost impossible to express the limits explicitly based on any known form of the spectral function and get a reasonably sharp result. Consequently, the only result using (5.2) to date was produced numerically. From a practical point of view, it would be desirable to express the skewness in a simpler, explicit form in terms of some parameters that would also convey physical insight. The empirical relationship given in equation (5.1) does fit this requirement because both Phillips (1961) and Longuet-Higgins (1963) showed that the deviation from the Gaussian distribution of a wave field would be due to the weakly nonlinear interaction. Therefore the skewness would be proportional to the wave slope. In this section, we are going to evaluate the theoretical bounds of K_3 based on (5.2) and a simplified Wallops spectral model. The result will be expressed explicitly in terms of an internal parameter, the significant slope of the wave field.

The simplified spectrum to be used is

$$\phi(n) = \begin{cases} \dfrac{\beta g^2}{n^m n_0^{5-m}}, & n \geqslant n_0, \\ 0, & n < n_0. \end{cases} \tag{5.4}$$

The relationship between this simplified spectral model and that of the full Wallops spectrum is equivalent to that of the simplified Phillips (1958) spectrum to the Pierson–Moskowitz spectrum (1964).

Before we start to use this simplified spectral model given in equation (5.4), we have to determine the coefficients and compare the properties of this model with the full Wallops spectrum.

The m value in (5.4) is still given by equation (2.4). But the β is different from that given in (2.11)). If we impose the constraint of the total energy content, then

$$\overline{\zeta^2} = \int \phi(n)\, dn = \frac{\beta g^2}{n_0^4} \frac{1}{m-1}. \tag{5.5}$$

Hence with the help of the dispersive relationship,

$$\beta = (m-1)\,(2\pi\S)^2. \tag{5.6}$$

Values of β determined experimentally are compared with the calculated ones from both (2.11) and (5.6). The results are shown in figure 5. The agreement between the experimental results and (5.6) is quite good, though the values given by (2.11) seem better. Now if we force m to be 5, then (5.6) would give the exact value of β as in the JONSWAP result shown in equation (4.4) as discussed earlier.

Next, we shall compare the spectrum bandwidth, ν, of the simplified spectrum with data and the full Wallops spectrum. Using the spectrum form in (5.4), one can easily show that the ith moment of the spectrum is

$$M_i = M_0 n_0^i \frac{m-1}{m-i-1},$$

where $M_0 = \overline{\zeta^2}$ is the zeroth moment. Then it follows that

$$\nu = \left(\frac{\mu_2}{M_2}\right)^{\frac{1}{2}} = \left\{1 - \frac{(m-1)(m-3)}{(m-2)^2}\right\}^{\frac{1}{2}} = \frac{1}{m-2}, \tag{5.7}$$

where μ_2 is the second central moment of the spectrum.

The values of ν calculated according to (5.7) are also given in figure 7. The agreement with the simplified model seems to be the best; even better than the full Wallops spectrum. But this fact alone should not be taken as the proof of the superiority of the simplified model. There are other criteria, too, as discussed previously. Even on this particular aspect, there are possible corrections that may influence the final outcome. For example, the unknown surface drift current effect has not been considered. The surface drift could shift the apparent frequency of the laboratory waves to higher frequency, thus giving a higher significant slope. With a rough estimation of the surface drift at $\frac{1}{2}u_*$ as reported by Wu (1975), the data points would be shifted slightly toward the curve predicted by the full spectral model. For lack of the direct surface drift data, this correction was not attempted here. Further studies are needed.

Based on the above discussion, we concluded that the simplified spectrum would still offer a good model accurate enough for most applications. It satisfies the total-energy-content requirement, and models correctly the spectral bandwidth. Thus it would give an acceptable spectral form, too. The most appealing feature of this simplified spectral function is its extremely simple form which allows it to be used in complicated calculations while still yielding explicit analytic results. Now, we will adopt this form for the skewness calculation.

As stated earlier, the bounds of the skewness of the probability distribution of the wave elevation were established by Longuet-Higgins (1963) as given in (5.2) and (5.3).

Now, if we use (5.4) as the spectral function, then, after some algebra, we get

$$\begin{aligned} I &= 12\int_0^\infty \left[\int_0^{n'} \frac{n^2}{g}\phi(n)\,dn\right]\phi(n')\,dn' \\ &= \frac{6\beta^2 g^3}{n_0^6(m-1)(m-2)}. \end{aligned} \tag{5.8}$$

Thus by combining (5.5) and (5.8), we have

$$L = 12\pi\S\frac{(m-1)}{(m-2)}. \tag{5.9}$$

Finally, from (5.2) we should have

$$5{\cdot}28\pi\S\frac{(m-1)}{(m-2)} \leqslant K_3 \leqslant 12{\cdot}12\pi\S\frac{(m-1)}{(m-2)}. \tag{5.10}$$

The values of K_3 calculated from (5.10) together with the observed data are given in figure 8. Because the m values are always larger than 5, it follows that the maximum value of the factor $(m-1)/(m-2)$ is only 1·25. Usually this factor has a value very close to unity. Thus the empirically determined value of skewness given in (5.1) is almost right at the middle of the bounds. So are the observational data points. The agreement is excellent.

It would be impossible to improve the sharpness of these bounds without a further consideration of the directional properties of the wave spectrum. For lack of such information, we submit that the empirical formula proposed by Huang & Long (1980)

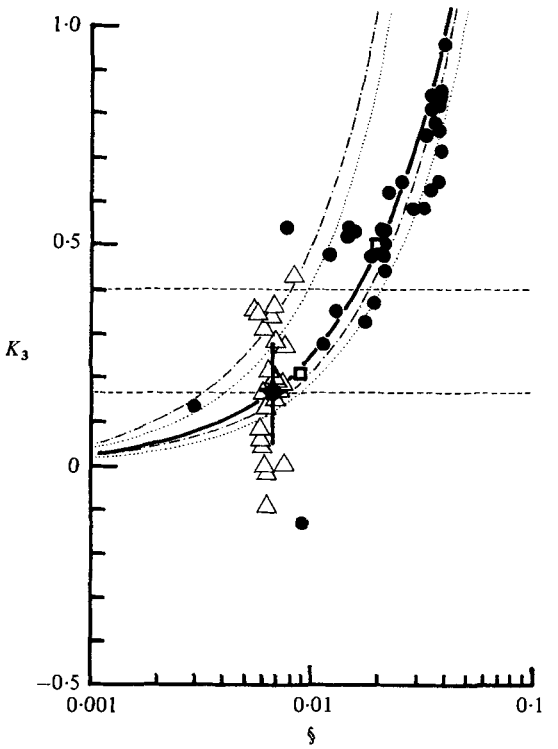

FIGURE 8. Comparisons of the observational data and the theoretical bounds of K_3. ●, laboratory data, Huang & Long (1980); △, field data by Kinsman (1960); ◆, the average value of Kinsman data, with one-sigma error bar; □, the remotely sensed data from GEOS-3 by Walsh (1979). ——, the empirical relationship of Huang & Long (1980); · · · · ·, the bounds by equation (5.10); - - - - - -, the bounds by equation (5.12); –·–·–, and the bound by equation (5.16).

is well supported by the theoretical bounds, and therefore could be used for practical applications with confidence.

Additional comparisons of the skewness bounds can be added by using other spectral models. This exercise is not intended to improve the accuracy or the sharpness of the bounds. Rather, the comparisons offer indirect tests of the sensitivity of the limits as given in (5.2) and the spectral model used. For example, the bounds can be calculated from the spectral model given in (1.1) with a constant value for β. Then

$$L = 4\beta^{\frac{1}{2}}. \tag{5.11}$$

If we choose $\beta = 10^{-2}$ as the mean value of β for the field data (see Phillips 1977), we should get

$$0{\cdot}176 \leqslant K_3 \leqslant 0{\cdot}404. \tag{5.12}$$

These bounds are rather poor even for the field data. The most crucial deficiency of these constant-valued bounds is not that they do not fit the data; rather, it is because they fail to offer any distinction among different sea states. If we relax the restriction on the constancy of β and adopt a variably valued function in terms of an internal variable §, the bounds could be improved substantially. For example, if we use the value of β as shown in equation (4.4) which is almost equal exactly to that given in (5.6) with $m = 5$, then the bounds for K_3 would be

$$7{\cdot}04\pi\S \leqslant K_3 \leqslant 16{\cdot}16\pi\S. \tag{5.13}$$

This result is also shown in figure 8. While (5.13) does dramatically improve the agreement with respect to a fixed value of β, the agreement is still not so good and so sharp as that given by (5.10). This seems to suggest the following facts. First, the spectral model is better if the Phillips coefficient is allowed to vary as a function of the internal variable, §, rather than stay as a constant. Secondly, the spectral model is better if the high-frequency slope of the spectrum is also allowed to vary. Thus, this simple application of the Wallops spectrum also serves as an indirect proof of the many advantages of the internal variable parametrization scheme and the resulting spectral model.

6. Conclusion

Based on the conclusion of the theoretical study by Hasselmann (1962, 1963*a*, *b*) and some laboratory studies, we proposed a wave spectral model that depends only on two internal parameters, § and n_0, with the significant slope § as a measure of the nonlinearity of the waves in the field. This spectral model has the properties of variable bandwidth, correct energy content and no empirical coefficients to be determined by the users. The form is simple.

One novel feature of the Wallops spectrum is the possibility of using remotely sensed data as an input directly. This remote-sensing approach, however, cannot be easily adopted for other spectral models. Admittedly, back-scattering measurements of wind are also available. But in order to use other models, information on fetch and duration are also necessary. Such parameters are difficult to define even under ideal conditions. At present, there is no reliable quantitative relationship available to define the various parameters needed for other spectral models other than some empirical relationships discussed earlier. Thus we feel that the Wallops spectral function offers a unique possibility of using the remote-sensing technology directly.

If one chooses, however, to rely on empirical relationships, then this spectral model, though not depending on external variables, can also be used to make wave predictions. Here we have to know how § and n_0 change with wind, fetch, etc. Such relationships exist in various empirical forms for fetch-limited cases as in Hasselmann *et al.* (1976), and Phillips (1977). Unfortunately, general formulae that also include decaying cases are still unavailable. Additional work is necessary in this area.

We should like to express our gratitude to our colleagues Messrs McGoogan and Parsons and Dr Walsh for their stimulating discussions. C-C.T. and Y.Y. are supported in part by NASA Contract NAS6-3018, and L.F.B. by NASA Contract NAS6-2940. This study is part of the NASA Supporting Research Technology Program.

REFERENCES

BURLING, R. W. 1959 The spectrum of wave at short fetches. *Dtsch. Hydrogr. Z.* **12**, 45–64, 96–117.

ELLIOTT, J. A. 1972 Microscale pressure fluctuations near waves being generated by the wind. *J. Fluid Mech.* **54**, 427–448.

HASSELMANN, K. 1962 On the non-linear energy transfer in a gravity wave spectrum. Part 1. *J. Fluid Mech.* **12**, 481–500.

HASSELMANN, K. 1963*a* On the non-linear energy transfer in a gravity wave spectrum. Part 2. *J. Fluid Mech.* **15**, 273–81.

HASSELMANN, K. 1963*b* On the non-linear energy transfer in a gravity wave spectrum. Part 3. *J. Fluid Mech.* **15**, 385–398.

HASSELMANN, K. 1973 Measurements of wind wave growth and swell decay during the Joint North Sea Wave Project (JONSWAP). *Herausgegeben von Deutsch. Hydrograph. Inst.*, Reihe A, no. 12.

HASSELMANN, K., ROSS, D. B., MÜLLER, P. & SELL, W. 1976 A parametric wave prediction model. *J. Physical Oceanog.* **6**, 200–228.

HICKS, B. L. 1960 The energy spectrum of small wind waves. *Univ. Illinois, C.S.L. Rep.* no. M-91.

HUANG, N. E. & LONG, S. R. 1980 An experimental study of the surface elevation probability distribution and statistics of wind generated waves. *J. Fluid Mech.* **101**, 179–200.

HUANG, N. E. & TUNG, C. C. 1976 The dispersion relation for a nonlinear random gravity wave field. *J. Fluid Mech.* **75**, 337–345.

IMASATO, N. 1976 Some characteristics of the development process of the wind-wave spectrum. *J. Oceanog. Soc. Japan* **32**, 27–32.

KINSMAN, B. 1960 Surface waves at short fetches and low wind speed – A field study. *Chesapeake Bay Inst. Johns Hopkins Univ. Tech. Rep.* no. 19.

KITAIGORODSKII, S. A. 1962 Applications of the theory of similarity to the analysis of wind-generated wave motion as a stochastic process. *Izv. Geophys. Ser. Acad. Sci. U.S.S.R.* **1**, 105–117.

LIU, P. C. 1971 Normalized and equilibrium spectra of wind waves on Lake Michigan. *J. Phys. Oceanog.* **1**, 249–257.

LONGUET-HIGGINS, M. S. 1957 The statistical analysis of a random, moving surface. *Phil. Trans. Roy. Soc.* A **249**, 321–387.

LONGUET-HIGGINS, M. S. 1962 The statistical geometry of random surfaces. *Hydrodynamic Stability: Proc. 13th Symp. Appl. Math., Providence, R.I.*, pp. 105–143. Amer. Math. Soc.

LONGUET-HIGGINS, M. S. 1963 The effect of non-linearities on statistical distributions in the theory of sea waves. *J. Fluid Mech.* **17**, 459–480.

LONGUET-HIGGINS, M. S. 1980 On the distribution of the heights of sea waves: some effects of nonlinearity and finite band width. *J. Geophys. Res.* **85**, 1519–1523.

LONGUET-HIGGINS, M. S., CARTWRIGHT, D. E. & SMITH, N. D. 1963 Observations of the directional spectrum of sea waves using the motions of a floating buoy. *Ocean Wave Spectra*, pp. 111–136. Prentice-Hall.

MCGOOGAN, J. T. 1975 Satellite altimetry applications. *I.E.E.E. Trans.* MTT-23, pp. 970–978.

MITSUYASU, H. 1968 On the growth of the spectrum of wind-generated waves (I.). *Rep. Res. Inst. Appl. Mech., Kyushu Univ.* **16** (55), 459–482.

MITSUYASU, H., TASI, F., SUHARA, T., MIZUNO, S., OHKUSU, M., HONDA, T. & RIKIISHI, K. 1980 Observation of the power spectrum of ocean waves using a cloverleaf buoy. *J. Phys. Oceanog.* **10**, 286–296.

MÜLLER, P. 1976 Parametrization of one-dimensional wind wave spectra and their dependence on the state of development. *Hamburger geophysikalische Einzelschriften*, Heft 31. Hamburg: G. M. L. Wittenborn Söhne.

PARSONS, C. L. 1979 GEOS-3 wave height measurements: an assessment during high sea state conditions in the north Atlantic. *J. Geophys. Res.* **84**, 4011–4020.

PHILLIPS, O. M. 1958 The equilibrium range in the spectrum of wind generated waves. *J. Fluid Mech.* **4**, 426–434.

PHILLIPS, O. M. 1960 On the dynamics of unsteady gravity waves of finite amplitude. Part 1. *J. Fluid Mech.* **9**, 193–217.

PHILLIPS, O. M. 1961 On the dynamics of unsteady gravity waves of finite amplitude. Part 2. *J. Fluid Mech.* **11**, 143–155.

PHILLIPS, O. M. 1977 *The Dynamics of the Upper Ocean.* Cambridge University Press.

PIERSON, W. J. 1962 The directional spectrum of a wind generated sea as determined from data obtained by the stereo wave observation project. *Coll. Engng N.Y.U. Met.* Paper 2, no. 6.

PIERSON, W. J. & MOSKOWITZ, L. 1964 A proposed spectral form for fully developed wind sea based on the similarity theory of S. A. Kitaigorodskii. *J. Geophys. Res.* **69**, 5181–5190.

SUTHERLAND, A. J. 1968 Growth of spectral components in a wind-generated wave train. *J. Fluid Mech.* **33**, 545–560.

TICK, L. J. 1959 A non-linear random model of gravity waves. Part 1. *J. Math. Mech.* **8**, 643–652.

TOBA, Y. 1973 Local balance in the air–sea boundary processes. III. On the spectrum of wind waves. *J. Oceanog. Soc. Japan* **29**, 209–220.

WALSH, E. J. 1979 Extraction of ocean wave height and dominant wave length from GEOS-3 altimeter data. *J. Geophys. Res.* **84**, 4003–4010.

WU, J. 1975 Wind-induced drift currents. *J. Fluid Mech.* **68**, 49–70.

WU, H.-Y., HSU, E. U. & STREET, R. L. 1977 The energy transfer due to air input, non-linear wave–wave interaction, and whitecap dissipation associated with wind generated waves. *Stanford Univ., Dept. Civil Engng Tech. Rep.* 207.